


Article

Aggregation-Induced Emission-Active Iridium(III) Complexes for Sensing Picric Acid in Water

Ping He ¹, Yan Chen ¹, Xiao-Na Li ², Ying-Ying Yan ¹ and Chun Liu ^{1,*} 

¹ State Key Laboratory of Fine Chemicals, Frontier Science Center for Smart Materials, School of Chemical Engineering, Dalian University of Technology, Dalian 116024, China

² School of Environmental Science and Technology, Key Laboratory of Industrial Ecology and Environmental Engineering (MOE), Dalian University of Technology, Dalian 116024, China

* Correspondence: cliu@dlut.edu.cn; Tel.: +86-411-84986182

Abstract: Herein, two new iridium(III) complexes, namely **Ir2** and **Ir3**, with a phenyl or triphenylamine (TPA) moiety at the 4-position of the phenyl ring at 2-phenylbenzothiazole, have been synthesized, and their emission properties have been studied systematically compared with the non-substituted complex **Ir1**. These three complexes exhibit aggregation-induced emission (AIE) in H₂O/CH₃CN. The TPA-substituted complex **Ir3** shows the highest AIE activity. All complexes can be used as sensors to detect picric acid (PA) in water. The Stern–Volmer constant (K_{SV}) of **Ir3** for the detection of PA was determined to be $1.96 \times 10^6 \text{ M}^{-1}$, with a low limit of detection of 2.52 nM. Proton nuclear magnetic resonance spectra, high-resolution mass spectrometry analysis, and density function theory calculations confirm that the emission quenching mechanism of **Ir3** is caused by photo-induced electron transfer. Furthermore, the efficient detection of PA in natural water proves that **Ir1–Ir3** can be used as promising sensors in the natural environment. These results suggest that the AIE-active iridium(III) complexes can be used to detect PA under environment-friendly conditions.

Keywords: Ir(III) complex; aggregation-induced emission; picric acid; aqueous media



Citation: He, P.; Chen, Y.; Li, X.-N.; Yan, Y.-Y.; Liu, C.

Aggregation-Induced Emission-Active Iridium(III) Complexes for Sensing Picric Acid in Water. *Chemosensors* **2023**, *11*, 177. <https://doi.org/10.3390/chemosensors11030177>

Academic Editors: Stefano Cinti, Valeria Gabrielli and Marco Frasconi

Received: 6 February 2023

Revised: 23 February 2023

Accepted: 27 February 2023

Published: 6 March 2023



Copyright: © 2023 by the authors. Licensee MDPI, Basel, Switzerland. This article is an open access article distributed under the terms and conditions of the Creative Commons Attribution (CC BY) license (<https://creativecommons.org/licenses/by/4.0/>).

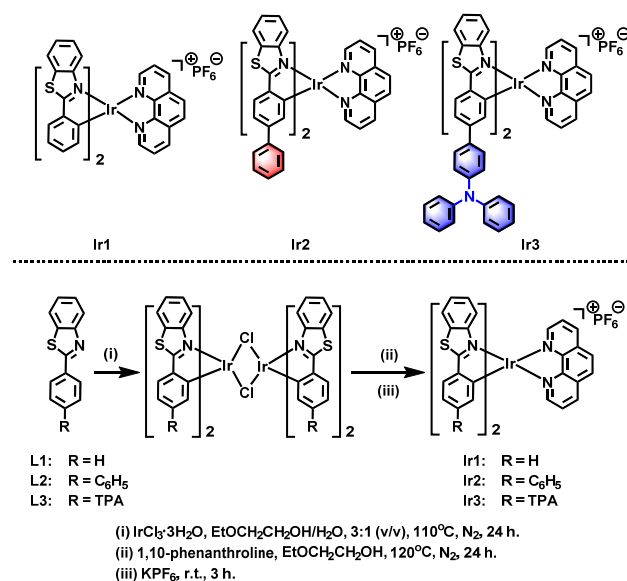
1. Introduction

Among nitroaromatics, picric acid (PA) containing three nitro groups shows superior explosive power and is extensively used to manufacture high explosives, which are a severe threat to society, human life, and property [1–3]. Additionally, PA plays an essential role in the leather, fuel manufacturing, pesticide, chemical fiber, pharmaceutical, and dye industries [4,5]. At the same time, a large amount of wastewater containing PA produced during its manufacturing, carriage, and utilization may cause water and soil pollution [6]. Therefore, it is highly desirable to develop a sensitive and selective detection method for PA.

Various analytical methods have been developed for explosives detection, including mass spectrometry [7], electrochemical methods [8], quartz crystal microbalance [9], and surface-enhanced Raman scattering [10]. However, these techniques usually need complex sample pretreatment and expensive and sophisticated instrumentation. In contrast, photoluminescence has been demonstrated to be an ideal analytical tool for trace explosives detection owing to its high sensitivity, operational simplicity, and real-time monitoring capability [11–14]. However, common luminescent materials frequently suffer from weak luminescence at the solid or aggregated states owing to aggregation-caused quenching (ACQ), which limits the detection of PA in aqueous media. Notably, the aggregation-induced emission (AIE) concept proposed by Ben Zhong Tang and coworkers effectively solves the ACQ problem [15]. Subsequently, many compounds with AIE activities have been designed and synthesized for PA detection [16–20]. Cyclometalated Ir(III) complexes

have numerous advantages, such as large Stokes shifts, high photoluminescence quantum yields, long lifetimes, and adequate stability [21–23]. Therefore, the development of AIE-active Ir(III) complexes for the detection of PA has become a research focus. However, most Ir(III) complexes reported for the detection of PA are based on 2-phenylpyridine (ppy), 1-phenylpyrazole (ppz), and their derivatives as cyclometalating ligands [24]. More importantly, the relationship between the AIE activity of an Ir(III) complex and its detection efficiency of PA is still elusive.

Although the AIE effect effectively settles the problems of weak emission or emission quenching of the luminescent materials [25] in the water medium caused by the ACQ influence and has made great progress rapidly, it is still a great challenge to control the AIE activity of the luminescent materials. In AIE systems, the most extensively accepted mechanism is the restriction of intramolecular rotations (RIR), which can block the non-radiative pathway and open up the radiative channel. Generally, propeller-like or rotor-like substituents are often used to activate the AIE property of the luminophores [26]. The nonplanar structure of triphenylamine (TPA) makes it an ideal building block for AIE-active luminophores. In addition, TPA exhibits strong electron-donating properties. Luminescent materials containing a TPA moiety facilitate interaction with electron-withdrawing nitroaromatic compounds [27–29]. Very recently, we found that the introduction of a diphenylamino group into the cyclometalating ligand significantly improved the detection efficiency of PA of the corresponding Ir(III) complex [30]. In order to systematically understand the effect of the molecular structure on AIE activity, in this work, two novel AIE-active cationic Ir(III) complexes, namely **Ir2** and **Ir3** with 2-phenylbenzothiazole derivatives as cyclometalating ligands, have been designed and synthesized (Scheme 1). This substantially broadens the structural diversity of the cyclometalating ligands that are not restricted to ppy or ppz-based ligands. By altering the substituent (phenyl or TPA) at the cyclometalating ligand, the regulation and enhancement of the AIE activities of the Ir(III) complexes have been realized compared with a non-substituted **Ir1**. Notably, the interaction of Ir(III) complexes with PA can effectively quench their luminescence, facilitating the eminently selective and sensitive detection of PA in a water medium. Moreover, the AIE activities of the Ir(III) complexes are positively correlated with the detection efficiencies of PA. These results provide a new idea for designing AIE-active Ir(III) complexes for PA detection.



Scheme 1. Structures and synthetic routes of cationic Ir(III) complexes.

2. Materials and Methods

2.1. Materials and Measurements

Unless otherwise stated, all the raw materials were commercially bought and have not been further purified. The solvents were handled according to requirements before use. Cyclometalating ligands (**L2** and **L3**) were prepared following the reported methods [31]. Proton nuclear magnetic resonance (^1H NMR) spectra were recorded using a 400 MHz Varian Unity Inova spectrophotometer. Carbon-13 nuclear magnetic resonance (^{13}C NMR) spectra were recorded using a 500 MHz Bruker AVANCE III spectrophotometer. High-resolution mass spectrometry (HRMS) was recorded using an Agilent-G6224 or an LTQ Orbitrap XL spectrometer equipped with an ESI source in a positive model. Fourier-transform infrared (FT-IR) spectra were recorded by Nicolet 6700 spectrometer using the KBr pellet method. The Ultraviolet-visible (UV-vis) absorption spectra were recorded using a Lambda 750s spectrophotometer. The emission spectra were recorded using a HITACHI F-7000 fluorescence spectrophotometer. Photoluminescence quantum yields (Φ_{PL}) were calculated compared with $[\text{Ir}(\text{ppy})_2(\text{acac})]$ ($\Phi_{\text{PL}} = 0.34$ in CH_2Cl_2 , under deoxygenated conditions). Phosphorescence lifetimes were measured using an Edinburgh FLS920 spectrometer. Density function theory (DFT) calculations were performed by PBE0/genecp. The LanL2DZ basis set was applied for iridium atoms, while the 6-311++G** basis set was used to handle all other atoms. The polarizable continuum model (PCM) model was adopted to consider the solvent effects. All of these calculations were carried out with the Gaussian 16 C.01 procedures [32].

2.2. Synthesis of the Ir(III) Complexes

$\text{IrCl}_3 \cdot 3\text{H}_2\text{O}$ (0.200 mmol, 70.5 mg) was reacted with 2.50 equiv. cyclometalating ligands (0.500 mmol, **L1** 106 mg, **L2** 144 mg, and **L3** 227 mg) in a mixture of 2-ethoxyethanol and water (6.00 mL/2.00 mL) at 110 °C for 24 h under an N_2 atmosphere to obtain a cyclometalated iridium bridged-chloride dimer. In the case of no further depuration, the dimer and 1,10-phenanthroline (0.600 mmol, 108 mg) were added to 2-ethoxyethanol at 120 °C under nitrogen for 24 h. As it cooled to room temperature, a 10-fold excess of saturated KPF_6 solution was poured, and the reaction mixture was stirred for 3 h. After adding 15.0 mL of water, the mixture was extracted with CH_2Cl_2 (3×15.0 mL). The combined organic layers were dried over Na_2SO_4 . The solvent was removed by rotary evaporation, and the crude products were subjected to depuration by column chromatography (methanol/ dichloromethane = 1:100, *v/v*).

Ir1. Yield: 74%; a yellow solid. ^1H NMR (400 MHz, $\text{DMSO}-d_6$) δ 8.97–8.94 (m, 2H), 8.42–8.41 (m, 2H), 8.35 (s, 2H), 8.17–8.13 (m, 4H), 8.06 (d, $J = 7.6$ Hz, 2H), 7.30 (t, $J = 7.6$ Hz, 2H), 7.17 (t, $J = 7.6$ Hz, 2H), 7.00–6.91 (m, 4H), 6.40 (d, $J = 7.6$ Hz, 2H), 5.74 (d, $J = 8.4$ Hz, 2H). ^{13}C NMR (125 MHz, $\text{DMSO}-d_6$) δ 181.31, 151.19, 149.77, 148.51, 146.80, 140.18, 139.46, 132.89, 132.04, 131.16, 130.69, 128.35, 127.81, 127.43, 127.01, 125.86, 124.58, 123.19, 116.31. FT-IR (KBr, cm^{-1}): $\nu = 3057, 1581, 1469, 1447, 1407, 1298, 1267, 838, 754, 724, 557$. HRMS (ESI, *m/z*): calcd. for $\text{C}_{38}\text{H}_{24}\text{IrN}_4\text{S}_2$ [$\text{M} - \text{PF}_6$] $^+$, 793.1072; found 793.1072.

Ir2. Yield: 52%; a yellow solid. ^1H NMR (400 MHz, $\text{DMSO}-d_6$) δ 8.97 (d, $J = 8.0$ Hz, 2H), 8.54 (s, 2H), 8.37 (s, 2H), 8.20–8.13 (m, 6H), 7.47 (d, $J = 7.6$ Hz, 2H), 7.34–7.26 (m, 8H), 7.18 (d, $J = 5.2$ Hz, 4H), 6.96 (t, $J = 7.2$ Hz, 2H), 6.59 (s, 2H), 5.83 (d, $J = 8.4$ Hz, 2H). ^{13}C NMR (125 MHz, $\text{DMSO}-d_6$) δ 180.87, 151.52, 150.34, 148.60, 146.81, 143.08, 139.63, 139.47, 139.41, 131.24, 130.73, 130.40, 128.86, 128.38, 128.07, 127.94, 127.54, 127.51, 126.45, 125.89, 124.57, 122.17, 116.37. FT-IR (KBr, cm^{-1}): $\nu = 3055, 2038, 1583, 1461, 1426, 1263, 840, 757, 723, 557$. HRMS (ESI, *m/z*): calcd. for $\text{C}_{50}\text{H}_{32}\text{IrN}_4\text{S}_2$ [$\text{M} - \text{PF}_6$] $^+$ 945.1698; found 945.1701.

Ir3. Yield: 49%; a brown solid. ^1H NMR (400 MHz, $\text{DMSO}-d_6$) δ 8.97 (d, $J = 8.4$ Hz, 2H), 8.52–8.51 (m, 2H), 8.37 (s, 2H), 8.18–8.13 (m, 4H), 8.06 (d, $J = 8.0$ Hz, 2H), 7.43 (dd, $J = 8.0, 1.2$ Hz, 2H), 7.31–7.26 (m, 10H), 7.10–7.05 (m, 8H), 6.92 (dd, $J = 16.0, 7.6$ Hz, 10H), 6.79 (d, $J = 8.8$ Hz, 4H), 6.59 (d, $J = 1.6$ Hz, 2H), 5.79 (d, $J = 8.4$ Hz, 2H). ^{13}C NMR (125 MHz, $\text{DMSO}-d_6$) δ 180.72, 151.45, 150.37, 148.60, 147.34, 146.83, 146.60, 142.24, 139.45, 138.96, 132.29, 131.13, 130.73, 129.57, 129.41, 128.38, 127.86, 127.46, 127.23, 125.75, 124.47, 123.58,

122.11, 121.37, 116.26. FT-IR (KBr, cm^{-1}): $\nu = 3057, 3032, 2040, 1578, 1510, 1489, 1429, 1323, 1283, 840, 755, 724, 696, 557$. HRMS (ESI, m/z): calcd. for $\text{C}_{74}\text{H}_{50}\text{IrN}_6\text{S}_2 [\text{M} - \text{PF}_6]^+$ 1279.3168; found 1279.3169.

2.3. Preparation of Stock Solutions for AIE and Detection of PA

Stock solutions of Ir(III) complexes were prepared at a concentration of 0.10 mM in CH_3CN . Samples for testing the emission properties were prepared by adding different fractions of deionized water to solutions of Ir(III) complexes. The aqueous suspensions of Ir(III) complexes (10 μM) in $\text{H}_2\text{O}/\text{CH}_3\text{CN}$ with a water fraction (f_w) of 90% were placed in a volumetric flask. Each time, a 3.0 mL aqueous suspension of Ir(III) complexes (10 μM) was placed in a quartz cuvette. For sensing studies, the stock solution of PA (10 mM) was prepared in $\text{H}_2\text{O}/\text{CH}_3\text{CN}$ (9/1, v/v); after that, a further dilution was made with $\text{H}_2\text{O}/\text{CH}_3\text{CN}$ (9/1, v/v) to various concentrations such as 0.10 mM, 0.20 mM, 0.30 mM, 0.40 mM, 0.50 mM, 0.60 mM, 0.70 mM, 0.80 mM, 0.90 mM, 1.0 mM, 2.0 mM, 3.0 mM, 4.0 mM, 5.0 mM, 6.0 mM, 7.0 mM, as well as 8.0 mM, and PA was detected on this account. The emission properties of Ir(III) complexes were measured by adding PA (30 μL) at different concentrations to suspensions of the Ir(III) complexes (10 μM , 3.0 mL) in $\text{H}_2\text{O}/\text{CH}_3\text{CN}$ (9/1, v/v). For the selectivity measurement, other analytes (8.0 mM, including nitrobenzene (NB), nitromethane (NM), *m*-dinitrobenzene (1,3-DNB), phenol, 4-methoxyphenol (MEHQ), *p*-cresol, and *m*-cresol) were prepared under the same conditions. The selectivity experiments were conducted by adding the same doses of nitroaromatic compounds and non-nitroaromatic compounds (30 μL) into the Ir(III) complexes assay aqueous suspension. The competing experiments were implemented as follows: the emission spectra were collected when various analytes were dispersed to the suspension of Ir(III) complexes, followed by the addition of the same equivalent amount of PA. To detect natural water samples, tap water, river water, rainwater, and seawater were collected from the laboratory, the playground at Dalian University of Technology, Bohai (Dalian, China), and the Lingshui River (Dalian, China), respectively. The emission spectra of the Ir(III) complexes in different water samples after adding the PA (8.0 mM, 30 μL) were recorded.

3. Results and Discussion

3.1. Photophysical Properties

The UV-Vis absorption and the normalized emission spectra of the Ir(III) complexes (**Ir1–Ir3**) in dilute CH_2Cl_2 are displayed in Figure 1. The intense absorption bands of these Ir(III) complexes were observed at 250–350 nm and are associated with spin-allowed ligand-centered ($^1\pi-\pi^*$) transitions [33]. The weaker absorption bands of **Ir1** and **Ir2** observed within the following range of 380–500 nm are due to the mixing between the metal-to-ligand charge transfer ($^1\text{MLCT}$ and $^3\text{MLCT}$) and ligand-centered $^3\pi-\pi^*$ transitions, which is facilitated by enhanced spin-orbital coupling [34]. Clearly, **Ir3** exhibited intense absorption relative to **Ir1** and **Ir2**, which was attributed to the presence of an electron-donating TPA substituent on the cyclometalating ligands. The normalized emission spectra of Ir(III) complexes **Ir1–Ir3** in CH_2Cl_2 exhibited that the introduction of a phenyl or TPA substituent on the cyclometalating ligand results in a red-shift for **Ir2** (34 nm) and **Ir3** (74 nm) in comparison with an unsubstituted **Ir1**. Additionally, **Ir1** and **Ir2** showed obvious fine vibronic splitting features, indicating a large ligand-centered (^3LC) character (^3LC). However, this unstructured emission spectrum of **Ir3** may be owing to the distinct properties of the emitted excited states. **Ir3** involves more $^3\text{MLCT}/^3\text{LLCT}$ features than **Ir1** as well as **Ir2** [35]. The phosphorescence quantum yields (Φ_{PL}) in deoxygenated CH_2Cl_2 were 0.55 (**Ir1**), 0.20 (**Ir2**), and 0.05 (**Ir3**), respectively (Table 1). The low phosphorescence quantum yields of **Ir3** may be due to the rotational motion of the benzene ring in TPA, which helps dissipate excited state energy in the solution state. The lifetimes (τ) of **Ir1–Ir3** in degassed CH_2Cl_2 were 3.73, 4.81, and 10.36 μs at room temperature (see Supplementary Material, Figure S1 for the phosphorescence decay curves of **Ir1–Ir3**). These results indicate that introducing a phenyl or TPA substituent on the cyclometalating ligand results in prolonged phosphores-

cence lifetimes for **Ir2** and **Ir3** compared with **Ir1**. The radiative and nonradiative decay rates of these Ir(III) complexes in CH₂Cl₂ were calculated. The results were as follows (Table 1). The data demonstrate that the phenyl or TPA substituent has a critical impact on the modification of the photophysical properties of these Ir(III) complexes.

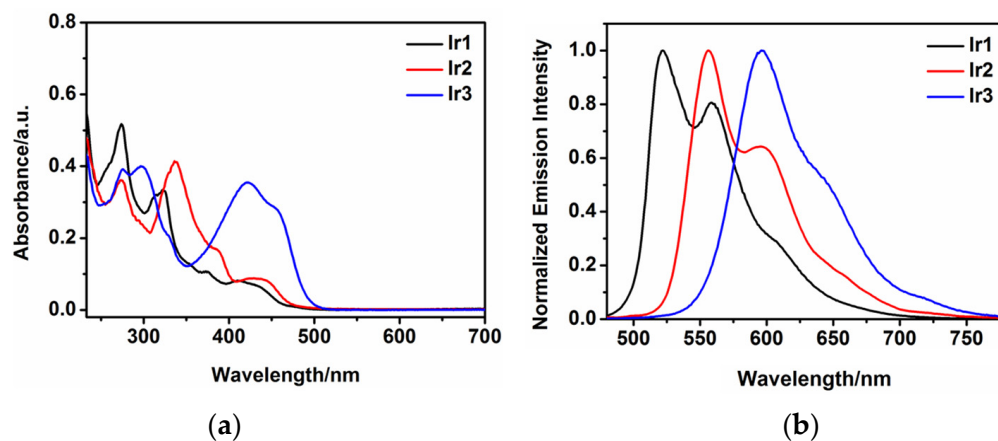


Figure 1. The UV-Vis absorption spectra (a) and normalized emission spectra (b) of **Ir1** (black), **Ir2** (red), and **Ir3** (blue) at room temperature (10 μ M in CH₂Cl₂).

Table 1. Photophysical data of Ir(III) complexes **Ir1–Ir3**.

Complex	λ_{abs}^a (nm)	λ_{em}^b (nm)	Φ_{PL}^c	τ^d (μ s)	k_r^e (10^6 s^{-1})	k_{nr}^e (10^6 s^{-1})
Ir1	274 (5.17)	522 , 559	0.55	3.73	0.148	0.120
	315 (3.21)					
	322 (3.34)					
	410 (0.81)					
Ir2	273 (3.61)	556 , 595	0.20	4.81	0.042	0.166
	336 (4.15)					
	423 (0.88)					
	423 (0.88)					
Ir3	275 (3.91)	596	0.05	10.36	0.005	0.092
	297 (4.00)					
	423 (3.55)					

^a Measured in CH₂Cl₂ at a concentration of 10 μ M and extinction coefficients ($10^4 \text{ M}^{-1} \text{ cm}^{-1}$) are shown in parentheses. ^b The maximum emission value is bold. ^c The quantum yields (Φ_{solution}) in deoxygenated CH₂Cl₂ were measured with [Ir(ppy)₂(acac)] ($\Phi_{\text{PL}} = 0.34$) as a standard. ^d In deoxygenated CH₂Cl₂ solution. ^e The radiative and nonradiative decay rates of k_r and k_{nr} were calculated from $k_r = \Phi_{\text{PL}} \times \tau^{-1}$, $k_{\text{nr}} = \tau^{-1} - k_r$.

3.2. AIE Activities

To evaluate the AIE activities of Ir(III) complexes **Ir1–Ir3**, their emissions were measured in H₂O/CH₃CN with water fractions in the range of 0–90%. As shown in Figure 2a–c, their emission intensities changed observably with various water contents in an H₂O/CH₃CN system, exhibiting a typical AIE phenomenon. Additionally, the maximum emission intensities of **Ir1–Ir3** were achieved at a water fraction of 90%, which is 1.9-, 3.5-, and 5.9-fold greater compared with those obtained in CH₃CN, respectively (Figure 2d). These results clearly demonstrate that phenyl or TPA substituent efficiently influences AIE activities. The enhanced AIE activity of **Ir2** relative to **Ir1** may be due to the introduction of a rotatable phenyl group. In a dilute solution, the rotatable phenyl group is active and serves as a relaxation channel for the excited states to deactivate. In the aggregated state, this phenyl group is restricted due to the physical constraint. This blocks the nonradiative pathway and thus enables the excitons to decay radiatively [26]. **Ir3** exhibits the highest AIE activity among the three complexes. It may be that the multiple benzene rings of **Ir3** contribute to the dissipation of the excited state energy through rotational motion. While in the aggregate, the motions become constrained, giving rise to intense luminescence.

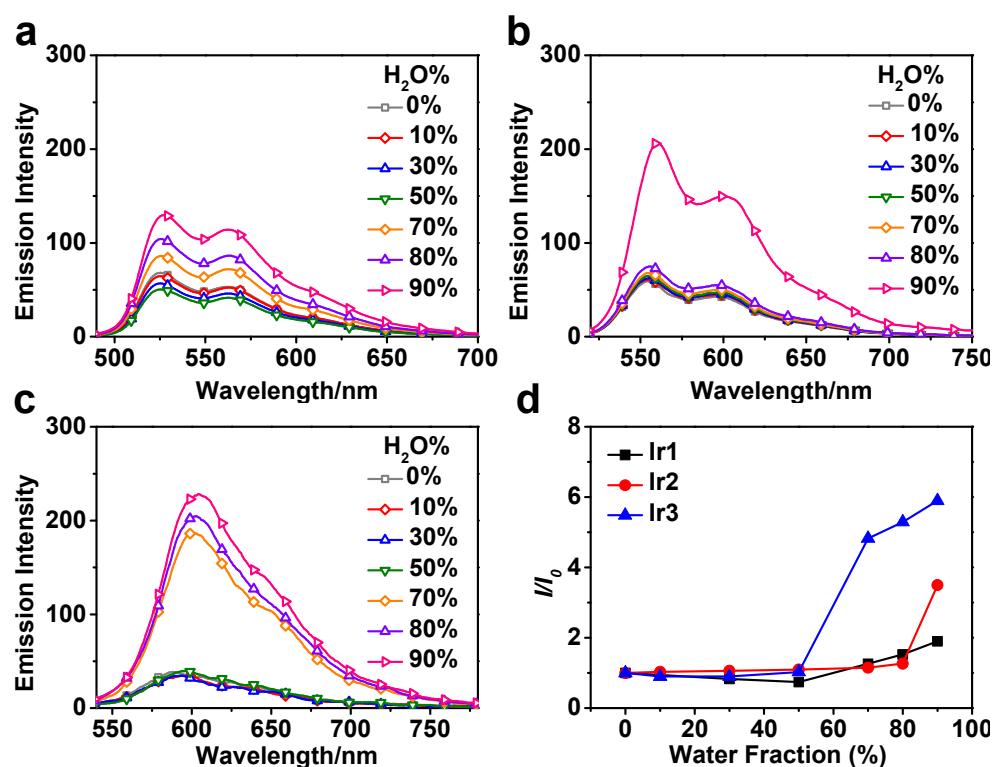


Figure 2. The emission spectra of Ir1 (a), Ir2 (b), and Ir3 (c) at 10 μ M in H₂O/CH₃CN with different H₂O fractions (0–90% *v/v*). (d) The relationship between the relative intensity of Ir1–Ir3 at the maximal emission wavelength and distinct water fractions. The excitation wavelengths of Ir1, Ir2, and Ir3 were 400 nm, 400 nm, and 440 nm, respectively.

3.3. Sensing of PA

The Ir(III) complexes with AIE activities available prevent luminescence quenching in a water medium. Thus, Ir(III) complexes Ir1–Ir3 were used as probes for PA detection in aqueous media. To explore the potential for application of these Ir(III) complexes as PA probes, the emission quenching experiments based on aqueous suspensions of Ir(III) complexes in H₂O/CH₃CN (*v/v* = 9:1, 10 μ M) toward different concentrations of PA were carried out. As can be seen from Figure 3c, upon the successive addition of PA (0 to 8.0 equiv.) to Ir3 in H₂O/CH₃CN (*v/v* = 9:1, 10 μ M), the luminescent intensities of Ir3 at 603 nm gradually decreased. The quenching was obviously found when 1.0 μ M of PA was added. As shown in Figure 3d, after adding PA (1.0 μ M), the quenching efficiency of Ir3 was close to 70%. Under the same conditions, just 6% and 37% of emission quenching efficiencies were observed for both Ir1 and Ir2, respectively. Until the concentration of PA reached 30 μ M, the quenching efficiency of Ir1 was over 70%, and when the PA concentration reached 80 μ M, negligible emission was identified with a high quenching efficiency of 97% for Ir3. With the aim of measuring the quenching constant of Ir3 toward PA, the Stern–Volmer plots of (I_0/I) vs. PA concentration were fit. The luminescence quenching influence was quantitatively analyzed by applying the Stern–Volmer (SV) equation: $I_0/I = K_{SV}[A] + 1$. The relative luminescent intensity (I_0/I) exhibits good linearity within the PA concentrations in the range of 0–6.0 μ M (Figure 3e), indicating that Ir3 can be applied as a probe for the quantitative detection of PA. The quenching constant (K_{SV}) was $1.96 \times 10^6 \text{ M}^{-1}$ for Ir3. Similarly, the luminescence of Ir1 and Ir2 was also quenched by PA in H₂O/CH₃CN (*v/v* = 9:1, 10 μ M), with quenching efficiencies of 94% and 95%, respectively (Figure 3a,b). The K_{SV} values of Ir1 and Ir2 were measured as $7.36 \times 10^4 \text{ M}^{-1}$ and $4.59 \times 10^5 \text{ M}^{-1}$, respectively. Furthermore, according to the literature reports [36,37], the limit of detection (LOD = $3\sigma/K$, σ represents the standard deviation of the blank measurement, and K represents the slope of the linear regression (see Figures S2 and S3 and Table S1) of Ir1–Ir3

for PA, which were measured as 50.17, 4.64, and 2.52 nM. The outcomes show that the AIE activities of these Ir(III) complexes **Ir1–Ir3** are positively correlated with the detection efficiencies of PA. Compared with the literature results, the sensitivities of **Ir2** and **Ir3** are either comparable or better than those of some reported sensors (see Table S2). It is worth noting that there is almost no change in the emission spectra in the detection process, thus demonstrating that no other emissive species formed during the quenching process.

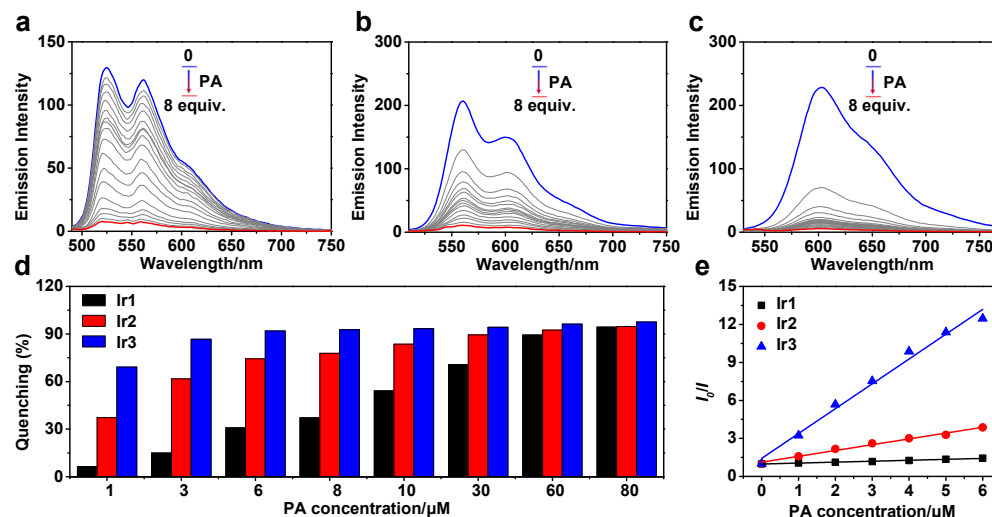


Figure 3. The emission spectra of **Ir1** (a), **Ir2** (b), and **Ir3** (c) at 10 μM in $\text{H}_2\text{O}/\text{CH}_3\text{CN}$ ($v/v = 9:1$) after adding different concentrations of PA. (d) The emission quenching efficiencies of **Ir1–Ir3** at different PA concentrations in $\text{H}_2\text{O}/\text{CH}_3\text{CN}$ ($v/v = 9:1$). (e) Plot of relative emission intensities (I_0/I , I = emission intensity and I_0 = emission intensity with no PA) versus PA concentrations in $\text{H}_2\text{O}/\text{CH}_3\text{CN}$ ($v/v = 9:1$). The excitation wavelengths of **Ir1**, **Ir2**, and **Ir3** were 400 nm, 400 nm, and 440 nm, respectively.

Based on the sensitive detection properties of Ir(III) complexes **Ir1–Ir3** for PA, the sensing selectivity of these Ir(III) complexes was also conducted in $\text{H}_2\text{O}/\text{CH}_3\text{CN}$ ($v/v = 9:1$, 10 μM). The phosphorescent emission quenching experiments for nitroaromatic and non-nitroaromatic compounds were studied, including picric acid (PA), nitromethane (NM), nitrobenzene (NB), and *m*-dinitrobenzene (1,3-DNB), as well as non-nitroaromatic compounds such as phenol, *m*-cresol, *p*-cresol, as well as 4-methoxyphenol (MEHQ). Compared with PA, all other analytes exhibited less of an effect on luminescence quenching under the same conditions (Figures 4a–c and S4), which can also be confirmed from the corresponding photos under a UV lamp at 365 nm (Figure 4a–c, inset). This might be because PA is a representative electron-deficient compound with three electron-withdrawing nitro groups. Ir(III) complexes **Ir1–Ir3** as electron donors can cause the photo-induced electron transfer (PET) for the emission quenching of **Ir1–Ir3** [38]. The results of selectivity experiments reveal that the Ir(III) complexes **Ir1–Ir3** have significantly high luminescent quenching efficiencies and selectivity for PA detection.

Anti-interference ability is another essential requirement for a suitable sensing probe. Thus, the influence of other potentially competitive analytes on PA detection was evaluated. As shown in Figure 4d–f and Figure S4, in the presence of other potential competitive analytes, PA can still significantly quench the emission of Ir(III) complexes **Ir1–Ir3** in $\text{H}_2\text{O}/\text{CH}_3\text{CN}$ ($v/v = 9:1$, 10 μM). These results demonstrate that Ir(III) complexes **Ir1–Ir3** have an excellent anti-interference ability toward PA detection over other analytes. Additionally, to assess the actual uses of Ir(III) complexes **Ir1–Ir3**, their luminescent responses for PA were evaluated in natural water samples made by tap water, river water, rainwater, and seawater. As shown in Figure 5a–c, the luminescence of Ir(III) complexes **Ir1–Ir3** is also quenched by PA in different samples of water/acetonitrile ($v/v = 9:1$). Additionally, the luminescence spectra of PA detected in the actual water samples do not change shape any

more compared with those in deionized water. As can be seen from Figure 5d, there is little difference in the quenching efficiency among different water samples. For example, the quenching efficiencies of Ir3 in tap water, river water, rainwater, and seawater were calculated to be 97%, 97%, 95%, and 96%, respectively, which are similar to those in deionized water. The results indicate that these Ir(III) complexes work well in natural water samples.

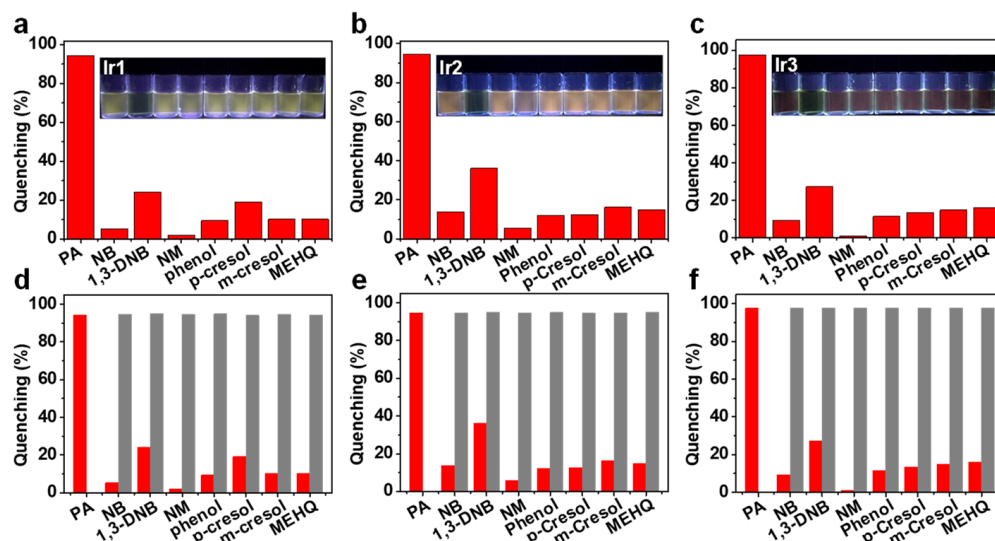


Figure 4. Quenching percentages for various analytes (8.0 equiv.) of Ir1 (a), Ir2 (b), and Ir3 (c) in H₂O/CH₃CN (*v/v* = 9:1, 10 μM). Inset: Photos showing the selectivity of Ir(III) complexes for detecting PA under UV lamp. Quenching percentages of Ir1 (d), Ir2 (e), and Ir3 (f) with other analytes (8.0 equiv.) in H₂O/CH₃CN (*v/v* = 9:1, 10 μM) before (red) and after (gray) the addition of 8.0 equivalent PA.

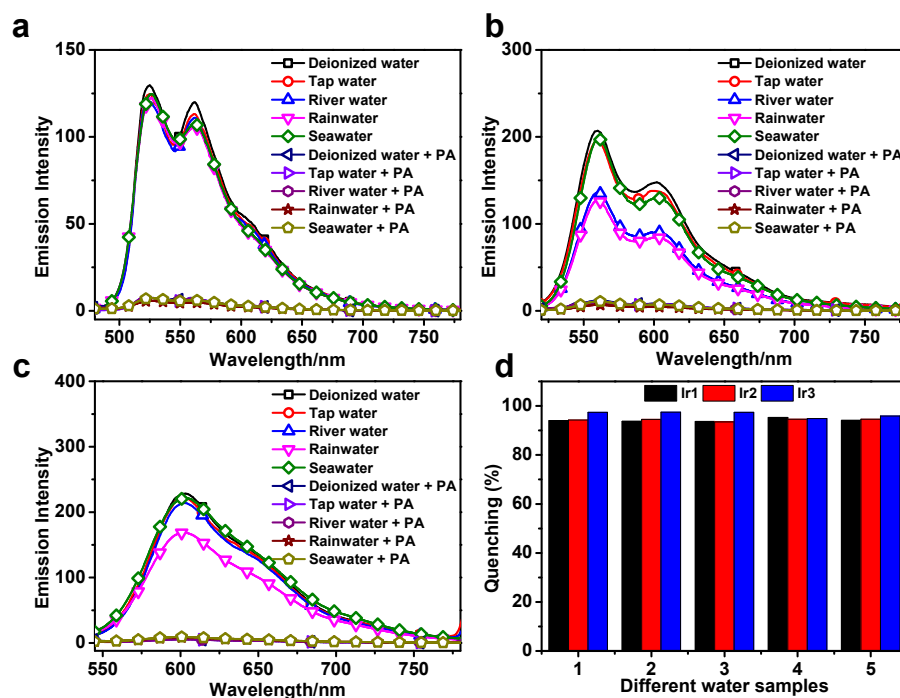


Figure 5. The luminescent responses of Ir1 (a), Ir2 (b), and Ir3 (c) at 10 μM toward PA in different water samples. (d) The quenching efficiency of Ir1–Ir3 in different water samples (1: deionized water, 2: tap water, 3: river water, 4: rainwater 5: seawater). The excitation wavelengths of Ir1, Ir2, and Ir3 were 400 nm, 400 nm, and 440 nm, respectively.

3.4. Mechanism for Sensing PA

To understand the emission quenching mechanism of the Ir(III) complexes for PA, **Ir3** was chosen to carry out the DFT calculations. The highest occupied molecular orbital (HOMO) and lowest unoccupied molecular orbital (LUMO) energy levels of **Ir3** were calculated. As shown in Figure 6, the LUMO energy of **Ir3** (−1.85 eV) is over that of PA (−2.59 eV), which contributes to electrons jumping to PA. Thus, the excited electron can transfer from the higher energy LUMO of **Ir3** to the lower energy LUMO of PA, leading to the photo-induced electron transfer-caused luminescence quenching of **Ir3**. The representative energy diagram shows that the energy gap of the adduct (**Ir3** + PA) (3.51 eV) is lower than that (4.49 eV) of **Ir3**, indicating that the adduct (**Ir3** + PA) is stable [39]. Additionally, the ¹H NMR spectra and HRMS of **Ir3** with and without PA were recorded, and they have almost identical spectra (Figure S5), demonstrating that **Ir3** does not decompose in the detection of PA. Therefore, the ¹H NMR spectra, HRMS analysis, and the DFT calculations suggest that the luminescence quenching process may be caused by PET.

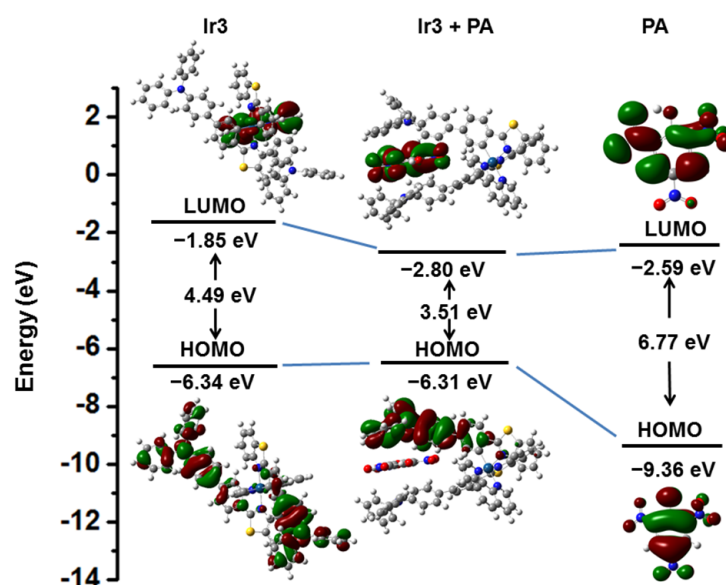


Figure 6. Calculated energy level diagram of **Ir3**, PA, and **Ir3** + PA.

4. Conclusions

In conclusion, two new AIE-active cationic Ir(III) complexes, namely **Ir2** and **Ir3**, with phenyl and TPA substituted cyclometalating ligands were synthesized and characterized, respectively. Compared with the non-substituted complex **Ir1**, **Ir2** and **Ir3** exhibit higher AIE activities. Ir(III) complexes **Ir1–Ir3** have been proved to be excellent chemosensors for the sensitive and selective detection of PA in water. The AIE activities of the complexes are positively correlated with their detection efficiencies of PA. Among them, **Ir3** exhibits the highest AIE activity as well as the highest quenching constant for detecting PA. The DFT calculations, ¹H NMR spectra, and HRMS analysis demonstrate that PET is responsible for the emission quenching in sensing PA. These findings provide novel insights into the design of high-performance Ir(III) complexes for the selective and sensitive detection of PA in water.

Supplementary Materials: The following supporting information can be downloaded at: <https://www.mdpi.com/article/10.3390/chemosensors11030177/s1>, Figure S1: Phosphorescence decay curves of **Ir1–Ir3**; Figures S2, S3, and Table S1: Calculation of limits of detection (LOD) of **Ir1–Ir3**; Table S2: A comparison of solvent, K_{SV} , and LOD for some sensors in detecting PA; Figure S4: Emission spectra of **Ir1–Ir3** in presence of different analytes; Figure S5: ¹H NMR spectra and HRMS of the cationic portion of **Ir3** before and after addition of PA. Figures S6–S17: NMR spectra, HRMS, and FT-IR spectra of **Ir1–Ir3** [27–29,40–43].

Author Contributions: Investigation, P.H.; data curation, P.H.; visualization, P.H.; validation, P.H.; writing—original draft, P.H.; formal analysis, P.H., Y.C., X.-N.L. and Y.-Y.Y.; conceptualization, C.L.; writing—review and editing, C.L.; funding acquisition, C.L.; project administration, C.L.; resources, C.L.; supervision, C.L. All authors have read and agreed to the published version of the manuscript.

Funding: This research was funded by financial support from the National Natural Science Foundation of China (21978042) and the Fundamental Research Funds for the Central Universities (DUT22LAB610).

Institutional Review Board Statement: Not applicable.

Informed Consent Statement: Not applicable.

Data Availability Statement: Not applicable.

Acknowledgments: The authors thank the High-Performance Computing Platform of Guangxi University for DFT calculations.

Conflicts of Interest: The authors declare no conflict of interest.

References

1. Liu, X.; Han, Y.; Shu, Y.; Wang, J.; Qiu, H. Fabrication and application of 2,4,6-trinitrophenol sensors based on fluorescent functional materials. *J. Hazard. Mater.* **2022**, *425*, 127987. [[CrossRef](#)] [[PubMed](#)]
2. Singh, P.; Mukherjee, A.; Mahato, A.; Pramanik, A.; Dhak, D. A review on chemoselective reduction of nitroarenes for wastewater remediation using biochar supported metal catalysts: Kinetic and mechanistic studies. *Chem. Afr.* **2022**. [[CrossRef](#)]
3. Ghasemi, F.; Hormozi-Nezhad, M.R. Determination and identification of nitroaromatic explosives by a double-emitter sensor array. *Talanta* **2019**, *201*, 230–236. [[CrossRef](#)] [[PubMed](#)]
4. Ghorai, P.; Hazra, A.; Mandal, J.; Malik, S.; Brandão, P.; Banerjee, P.; Saha, A. Selective low-level detection of a perilous nitroaromatic compound using tailor-made Cd(II)-based coordination polymers: Study of photophysical properties and effect of functional groups. *Inorg. Chem.* **2023**, *62*, 98–113. [[CrossRef](#)] [[PubMed](#)]
5. Ouyang, T.; Guo, X.; Cui, Q.; Zhang, W.; Dong, W.; Fei, T. Conjugated polymer nanoparticles based on anthracene and tetraphenylethene for nitroaromatics detection in aqueous phase. *Chemosensors* **2022**, *10*, 366. [[CrossRef](#)]
6. Zhu, C.; Huang, H.; Chen, Y. Recent advances in biological removal of nitroaromatics from wastewater. *Environ. Pollut.* **2022**, *307*, 119570. [[CrossRef](#)]
7. Zhang, Y.; Ma, X.; Zhang, S.; Yang, C.; Ouyang, Z.; Zhang, X. Direct detection of explosives on solid surfaces by low temperature plasma desorption mass spectrometry. *Analyst* **2009**, *134*, 176–181. [[CrossRef](#)] [[PubMed](#)]
8. Arman, A.; Sağlam, Ş.; Üzer, A.; Apak, R. Electrochemical determination of nitroaromatic explosives using glassy carbon/multi walled carbon nanotube/polyethyleneimine electrode coated with gold nanoparticles. *Talanta* **2022**, *238*, 122990. [[CrossRef](#)]
9. Larsson, A.; Angbrant, J.; Ekeröth, J.; Månsson, P.; Liedberg, B. A novel biochip technology for detection of explosives-TNT: Synthesis, characterisation and application. *Sens. Actuators B* **2006**, *113*, 730–748. [[CrossRef](#)]
10. Muehlethaler, C.; Leona, M.; Lombardi, J.R. Review of surface enhanced Raman scattering applications in forensic science. *Anal. Chem.* **2016**, *88*, 152–169. [[CrossRef](#)]
11. Sun, X.; Wang, Y.; Lei, Y. Fluorescence based explosive detection: From mechanisms to sensory materials. *Chem. Soc. Rev.* **2015**, *44*, 8019–8061. [[CrossRef](#)] [[PubMed](#)]
12. Wu, X.; Hang, H.; Li, H.; Chen, Y.; Tong, H.; Wang, L. Water-dispersible hyperbranched conjugated polymer nanoparticles with sulfonate terminal groups for amplified fluorescence sensing of trace TNT in aqueous solution. *Mater. Chem. Front.* **2017**, *1*, 1875–1880. [[CrossRef](#)]
13. Barata, P.D.; Prata, J.V. Fluorescent calix[4]arene-carbazole-containing polymers as sensors for nitroaromatic explosives. *Chemosensors* **2020**, *8*, 128. [[CrossRef](#)]
14. Dhiman, S.; Singla, N.; Ahmad, M.; Singh, P.; Kumar, S. Protonation-and electrostatic-interaction-based fluorescence probes for the selective detection of picric acid (2,4,6-trinitrophenol)—An explosive material. *Mater. Adv.* **2021**, *2*, 6466–6498. [[CrossRef](#)]
15. Luo, J.; Xie, Z.; Lam, J.W.Y.; Cheng, L.; Chen, H.; Qiu, C.; Kwok, H.S.; Zhan, X.; Liu, Y.; Zhu, D.; et al. Aggregation-induced emission of 1-methyl-1,2,3,4,5-pentaphenylsilole. *Chem. Commun.* **2001**, *18*, 1740–1741. [[CrossRef](#)] [[PubMed](#)]
16. Miao, C.; Li, D.; Zhang, Y.; Yu, J.; Xu, R. AIE luminogen functionalized mesoporous silica nanoparticles as efficient fluorescent sensor for explosives detection in water. *Microporous Mesoporous Mater.* **2014**, *196*, 46–50. [[CrossRef](#)]
17. Li, K.; Yu, R.-H.; Shi, C.-M.; Tao, F.-R.; Li, T.-D.; Cui, Y.-Z. Electrospun nanofibrous membrane based on AIE-active compound for detecting picric acid in aqueous solution. *Sens. Actuators B* **2018**, *262*, 637–645. [[CrossRef](#)]
18. Ma, Y.; Zhang, Y.; Liu, X.; Zhang, Q.; Kong, L.; Tian, Y.; Li, G.; Zhang, X.; Yang, J. AIE-active luminogen for highly sensitive and selective detection of picric acid in water samples: Pyridyl as an effective recognition group. *Dyes Pigm.* **2019**, *163*, 1–8. [[CrossRef](#)]
19. Kajjam, A.B.; Didar, S.; Allen, M.J. AIE active triphenylamine-CF₃ based α -cyanostilbenes for selective detection of picric acid in aqueous media and solid support. *J. Photochem. Photobiol. A* **2022**, *431*, 114036. [[CrossRef](#)]

20. Zan, Y.; Kang, Y.; Wang, B.; Cui, S.; Shen, Z.; Shu, J.; Kong, X.; Chen, L.; Yan, X.; Li, Y. Amphiphilic fluorescent nanospheres for quantitative sensing of trinitrophenol in water system. *Dyes Pigm.* **2022**, *202*, 110296. [CrossRef]
21. Chi, Y.; Chang, T.-K.; Ganesan, P.; Rajakannu, P. Emissive bis-tridentate Ir(III) metal complexes: Tactics, photophysics and applications. *Coord. Chem. Rev.* **2017**, *346*, 91–100. [CrossRef]
22. Aoki, S.; Yokoi, K.; Hisamatsu, Y.; Balachandran, C.; Tamura, Y.; Tanaka, T. Post-complexation functionalization of cyclometalated iridium(III) complexes and applications to biomedical and material sciences. *Top. Curr. Chem.* **2022**, *380*, 36. [CrossRef] [PubMed]
23. Schreier, M.R.; Guo, X.; Pfund, B.; Okamoto, Y.; Ward, T.R.; Kerzig, C.; Wenger, O.S. Water-soluble tris(cyclometalated) iridium(III) complexes for aqueous electron and energy transfer photochemistry. *Acc. Chem. Res.* **2022**, *55*, 1290–1300. [CrossRef] [PubMed]
24. Ramdass, A.; Sathish, V.; Thanasekaran, P. AIE or AIE(P)E-active transition metal complexes for highly sensitive detection of nitroaromatic explosives. *Results Chem.* **2022**, *4*, 100337. [CrossRef]
25. Xie, Z.; Sun, P.; Wang, Z.; Li, H.; Yu, L.; Sun, D.; Chen, M.; Bi, Y.; Xin, X.; Hao, J. Metal–Organic Gels from Silver Nanoclusters with Aggregation-Induced Emission and Fluorescence-to-Phosphorescence Switching. *Angew. Chem. Int. Ed.* **2020**, *59*, 9922–9927. [CrossRef]
26. Mei, J.; Leung, N.L.C.; Kwok, R.T.K.; Lam, J.W.Y.; Tang, B.Z. Aggregation-induced emission: Together we shine, united we soar! *Chem. Rev.* **2015**, *115*, 11718–11940. [CrossRef]
27. Sathiyam, G.; Balasubramaniam, B.; Ranjan, S.; Chatterjee, S.; Sen, P.; Garg, A.; Gupta, R.; Singh, A. A novel star-shaped triazine-triphenylamine-based fluorescent chemosensor for the selective detection of picric acid. *Mater. Today Chem.* **2019**, *12*, 178–186. [CrossRef]
28. Zhang, H.-J.; Tian, Y.; Tao, F.-R.; Yu, W.; You, K.-Y.; Zhou, L.-R.; Su, X.; Li, T.-D.; Cui, Y.-Z. Detection of nitroaromatics based on aggregation induced emission of barbituric acid derivatives. *Spectrochim. Acta Part A* **2019**, *222*, 117168. [CrossRef]
29. Verbitskiy, E.V.; Kvashnin, Y.A.; Baranova, A.A.; Khokhlov, K.O.; Chuvashov, R.D.; Schapov, I.E.; Yakovleva, Y.A.; Zhilina, E.F.; Shchepochkin, A.V.; Makarova, N.I.; et al. Synthesis and characterization of linear 1,4-diazine-triphenylamine-based selective chemosensors for recognition of nitroaromatic compounds and aliphatic amines. *Dyes Pigm.* **2020**, *178*, 108344. [CrossRef]
30. He, P.; Chen, Y.; Li, X.; Yan, Y.; Liu, C. AIPE-active cationic Ir(III) complexes for efficient detection of 2,4,6-trinitrophenol and oxygen. *Dalton Trans.* **2023**, *52*, 128–135. [CrossRef]
31. Rao, X.; Liu, C.; Qiu, J.; Jin, Z. A highly efficient and aerobic protocol for the synthesis of *N*-heteroaryl substituted 9-arylcarbazolyl derivatives via a palladium-catalyzed ligand-free Suzuki reaction. *Org. Biomol. Chem.* **2012**, *10*, 7875–7883. [CrossRef] [PubMed]
32. Frisch, M.J.; Trucks, G.W.; Schlegel, H.B.; Scuseria, G.E.; Robb, M.A.; Cheeseman, J.R.; Scalmani, G.; Barone, V.; Petersson, G.A.; Nakatsuji, H.; et al. *Gaussian 16*; Gaussian, Inc.: Wallingford, CT, USA, 2016. Available online: <https://gaussian.com/gaussian16> (accessed on 5 February 2023).
33. Jang, J.-H.; Park, H.J.; Park, J.Y.; Kim, H.U.; Hwang, D.-H. Orange phosphorescent Ir(III) complexes consisting of substituted 2-phenylbenzothiazole for solution-processed organic light-emitting diodes. *Org. Electron.* **2018**, *60*, 31–37. [CrossRef]
34. Lamansky, S.; Djurovich, P.; Murphy, D.; Abdel-Razzaq, F.; Lee, H.-E.; Adachi, C.; Burrows, P.E.; Forrest, S.R.; Thompson, M.E. Highly phosphorescent bis-cyclometalated iridium complexes: synthesis, photophysical characterization, and use in organic light emitting diodes. *J. Am. Chem. Soc.* **2001**, *123*, 4304–4312. [CrossRef]
35. Yu, H.; Liu, C.; Yu, Z.; Zhang, L.; Xiu, J. Effect of ancillary ligands on the properties of diphenylphosphoryl-substituted cationic Ir(III) complexes. *J. Mater. Chem. C* **2017**, *5*, 3519–3527. [CrossRef]
36. Das, P.; Mandal, S.K. Understanding the effect of an amino group on the selective and ultrafast detection of TNP in water using fluorescent organic probes. *J. Mater. Chem. C* **2018**, *6*, 3288–3297. [CrossRef]
37. Hao, H.; Xu, C.; Luo, H.; Yang, J.; Liu, C.; Xu, B.; Shi, G.; Xing, X.; Chi, Z. An AIE luminogen-based electropolymerized film: An ultrasensitive fluorescent probe for TNP and Fe³⁺ in water. *Mater. Chem. Front.* **2021**, *5*, 492–499. [CrossRef]
38. Cui, Y.; Wen, L.-L.; Shan, G.-G.; Sun, H.-Z.; Mao, H.-T.; Zhang, M.; Su, Z.-M. Di-/trinuclear cationic Ir(III) complexes: Design, synthesis and application for highly sensitive and selective detection of TNP in aqueous solution. *Sens. Actuators B* **2017**, *244*, 314–322. [CrossRef]
39. Yi, S.; Lu, Z.; Xie, Z.; Hou, L. Amphiphilic gemini-iridium (III) complex for rapid and selective detection of picric acid in water and intracellular. *Talanta* **2020**, *208*, 120372. [CrossRef]
40. Alam, P.; Kaur, G.; Kachwal, V.; Gupta, A.; Roy Choudhury, A.; Laskar, I.R. Highly sensitive explosive sensing by “aggregation induced phosphorescence” active cyclometalated iridium(III) complexes. *J. Mater. Chem. C* **2015**, *3*, 5450–5456. [CrossRef]
41. Wen, L.-L.; Hou, X.-G.; Shan, G.-G.; Song, W.-L.; Zhang, S.-R.; Sun, H.-Z.; Su, Z.-M. Rational molecular design of aggregation-induced emission cationic Ir(III) phosphors achieving supersensitive and selective detection of nitroaromatic explosives. *J. Mater. Chem. C* **2017**, *5*, 10847–10854. [CrossRef]

42. Hou, X.-G.; Wu, Y.; Cao, H.-T.; Sun, H.-Z.; Li, H.-B.; Shan, G.-G.; Su, Z.-M. A cationic iridium(III) complex with aggregation-induced emission (AIE) properties for highly selective detection of explosives. *Chem. Commun.* **2014**, *50*, 6031–6034. [[CrossRef](#)] [[PubMed](#)]
43. Che, W.; Li, G.; Liu, X.; Shao, K.; Zhu, D.; Su, Z.; Bryce, M.R. Selective sensing of 2,4,6-trinitrophenol (TNP) in aqueous media with “aggregation-induced emission enhancement” (AIEE)-active iridium(III) complexes. *Chem. Commun.* **2018**, *4*, 1730–1733. [[CrossRef](#)] [[PubMed](#)]

Disclaimer/Publisher’s Note: The statements, opinions and data contained in all publications are solely those of the individual author(s) and contributor(s) and not of MDPI and/or the editor(s). MDPI and/or the editor(s) disclaim responsibility for any injury to people or property resulting from any ideas, methods, instructions or products referred to in the content.